Miner Petrol (2010) 98:227–243
DOI 10.1007/s00710-009-0064-3

ORIGINAL PAPER

Petrogenesis of a basalt-comendite-pantellerite rock suite: the Boseti Volcanic Complex (Main Ethiopian Rift)

Fiorenzo Ronga · Michele Lustrino · Andrea Marzoli · Leone Melluso

Received: 26 January 2009 / Accepted: 11 June 2009 / Published online: 4 July 2009

Abstract Petrological and geochemical data for basic (alkali basalts and hawaiites) and silicic peralkaline rocks, plus rare intermediate products (mugearites and benmoreites) from the Pleistocene Boseti volcanic complex (Main Ethiopian Rift, East Africa) are reported in this work. The basalts are slightly alkaline or transitional, have peaks at Ba and Nb in the mantle-normalized diagrams and relatively low $^{87}Sr/^{86}Sr$ (0.7039–0.7044). The silicic rocks (pantellerites and comendites) are rich in sanidine and anorthoclase, with mafic phases being represented by fayalite-rich olivine, opaque oxides, aenigmatite and slightly Na-rich ferroaugite (ferrohedenbergite). These rocks were generated after prolonged fractional crystallization process (up to 90–95 %) starting from basaltic parent magmas at shallow depths and fO_2 conditions near the QFM buffer. The apparent Daly Gap between mafic and evolved Boseti rocks is explained with a model involving the silicic products filling upper crustal magma chambers and erupted preferentially with respect to basic and intermediate products. Evolved liquids could have been the only magmas which filled the uppermost magma reservoirs in the crust, thus giving time to evolve towards Rb-, Zr- and Nb-rich peralkaline rhyolites in broadly closed systems.

Editorial handling L.G. Gwalani

F. Ronga · L. Melluso (✉)
Dipartimento di Scienze della Terra,
Università degli Studi di Napoli Federico II,
Via Mezzocannone 8,
80134 Naples, Italy
e-mail: melluso@unina.it

M. Lustrino
Dipartimento di Scienze della Terra,
Università degli Studi di Roma La Sapienza,
P.le A. Moro 5,
00185 Rome, Italy

M. Lustrino
CNR Istituto di Geologia Ambientale e Geoingegneria (IGAG),
c/o Dipartimento di Scienze della Terra,
Università degli Studi di Roma La Sapienza,
P.le A. Moro 5,
00185 Rome, Italy

A. Marzoli
Dipartimento di Geoscienze,
Università degli Studi di Padova and IGG-CNR,
via Matteotti 30,
35100 Padova, Italy

Introduction

The East African Rift System (EARS) is a classical example of a young intra-continental rift (Fig. 1a; Chorowicz 2005). This rift developed during the Cenozoic accompanied by an intense magmatic activity in the form of huge volumes of basic magmas plus minor evolved products and almost no intermediate-SiO_2 compositions (Di Paola 1972; Trua et al. 1999; Peccerillo et al. 2003).

The source of the abundant mafic rocks has been alternatively identified with the lithospheric mantle (Rogers et al. 2000) or sub-lithospheric reservoirs, either the shallow asthenosphere (Mohr 1992; Chorowicz 2005 and references therein) or deep-seated mantle plume (Baker et al. 1998; Ebinger and Sleep 1998; George et al. 1998; Bertrand et al. 2003; Furman et al. 2004). Similarly, the origin of the evolved magmas (mostly trachytes and rhyolites) is attributed alternatively to fractional crystallization processes of basaltic parental magmas (e.g., Barberi et al. 1975), or to open system evolution, involving crustal assimilation, fractional crystallization and magma mixing (Barberio et al.

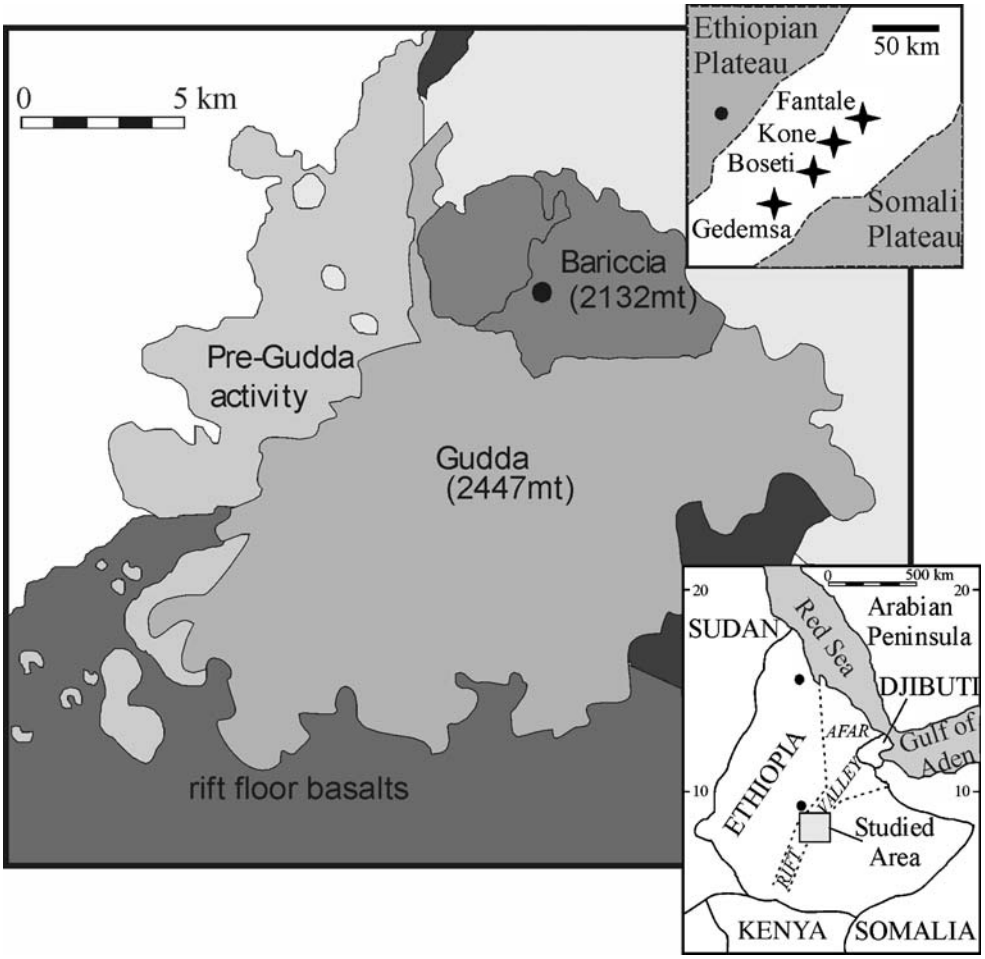

Fig. 1 Schematic geological map of Boseti volcanic complex (largely redrawn after Brotzu et al. 1980)

1999; Trua et al. 1999; Macdonald et al. 2008 and references therein).

In this study new mineral chemical and geochemical data for rocks of the Boseti Volcanic Complex in Ethiopia, sampled in fieldworks between 1970 and 1976 (Brotzu et al. 1974, 1978, 1980), are used to constrain the genesis of the Boseti magmas.

Geological setting

The Main Ethiopian Rift (MER) is bounded by the Afar depression to the North, the Gregory Rift (known also as the Kenya Rift) to the South, the Somali Plateau to the East and the Ethiopian Plateau to the West. The MER, along with the basaltic plateau, constitute the Ethiopian Igneous Province (Fig. 1). The crustal thickness measured along the rift axis varies from ~32 km in the central part of the northern MER to ~24 km south of Afar (Tessema and Antoine 2004). Moving off the rift axis, crustal thickness increases up to ~36–40 km below the rift shoulders and below the plateau (Tessema and Antoine 2004; Benoit et al. 2006).

The magmatic activity in Ethiopia started in the Oligocene (Berhe et al. 1987) and is divided in two main stages: a Pre-Rift stage and a Rift stage. The Pre-Rift stage is characterized by the eruption of Plateau successions presently covering more than 600,000 km^2 (Mohr and Zanettin 1988) and started with the emplacement of the Ashange Formation, made up of tholeiitic and mildly alkaline basalts. Whole rock K-Ar ages (Merla et al. 1979; Berhe et al. 1987) for this and the overlying Aiba Formation vary from ~60 Ma to ~30 Ma. The pre-Rift stage igneous activity continued with the emplacement of voluminous fissural basalts (Aiba Formation) followed by the emplacement of bimodal products (Alaji Formation), forming the Aiba-Alaji Group (~30–23 Ma; whole rock K-Ar and whole-rock and feldspar separate ^{40}Ar-^{39}Ar ages; Piccirillo et al. 1979; Brotzu et al. 1986; Berhe et al. 1987; Hofmann et al. 1997; Chernet et al. 1998; Zanettin et al. 2006). The Pre-Rift magmatic activity ended with the emplacement of Termaber Guassa and Termaber Megezez Formations of the Termaber Group, characterized by central-type volcanism ranging in composition from basalts to phonolites through rare intermediate products (~22–13 Ma; K-Ar whole-rock ages; Justin Visentin et al.

1974; Piccirillo et al. 1979; Berhe et al. 1987; Chernet et al. 1998).

The Rift stage is characterized by emplacement of fissural basalts belonging to the Anchar Formation (~12–10 Ma; whole-rock K-Ar ages; Brotzu et al. 1986; Woldegabriel et al. 1990; Chernet et al. 1998, and references therein), followed by the voluminous fissural volcanism of the Nazret Group (~9.5–5.8 Ma; whole-rock K-Ar ages; Di Paola 1972; Brotzu et al. 1986; Woldegabriel et al. 1990; Chernet et al. 1998). After the emplacement of the Nazret Group, mainly cropping out along the rift flanks, and including abundant evolved rocks and minor basic products, fissural volcanism became gradually confined to the present rift floor, with the emplacement of basalts of the Bofa Formation (~3.5–1.5 Ma; whole-rock K-Ar ages; Brotzu et al. 1986; Woldegabriel et al. 1990; Chernet et al. 1998).

From a tectonic point of view, two main fault systems have been identified in the MER: one with a N30-40°E trend, which characterizes the rift margins, and another with a N12°E to N20°E trend, with a left-lateral *en echelon* component which characterizes the rift floor (Boccaletti et al. 1998). This second fault system constitutes the Wonji Fault Belt (e.g., Chernet et al. 1998; Chorowicz 2005) which is associated with a basic fissural volcanism represented by the Wonji Group (~1.6–0.1 Ma; whole-rock ^{40}Ar-^{39}Ar and K-Ar ages; Brotzu et al. 1986; Woldegabriel et al. 1990; Chernet et al. 1998). Along the Wonji Foult Belt, many central volcanoes erupt mostly silicic products, often with peralkaline affinity, including Fantale, Kone, Gedemsa and the Boseti Volcanic Complex (e.g., Brotzu et al. 1980; Gibson 1974; Peccerillo et al. 2003; Furman et al. 2006a).

Volcanological background of the Boseti volcanic complex

The Boseti Volcanic Complex is located in the northern sector of MER and it is formed by the coalescence of two main volcanic edifices: Gudda (2,447 m a.s.l.) and Bariccia (2,132 m a.s.l.). Previous volcanological, geochemical and petrologic data on this volcanic complex were presented by Di Paola (1972) and Brotzu et al. (1974, 1980). According to these authors, the magmatic activity is grouped in three main stages: 1) the Pre-caldera activity, responsible for the formation of main volcanic edifice (old Gudda or pre-caldera Gudda); 2) Caldera formation, now recognizable only in the NW sector of the complex; 3) Post-caldera activity which led to the formation of the Gudda and Bariccia volcanoes (Fig. 1).

The activity of the Boseti Volcanic Complex started after fissural volcanism of the Balchi Formation (Post-Nazret Group) with the emplacement of pre-caldera volcanics and lateral activity eruptions. The pre-caldera (Pleistocene) rocks are represented by lava flows, spatter and cinder cones of basaltic composition and silicic lava flows of peralkaline rhyolitic composition. This stage ended with the emplacement of ashy and pumiceous falls of pantelleritic composition. The lateral activity (i.e., in peripheral areas compared to the main area of magma emission) of the pre-caldera Gudda is represented by domes and composite cones. At the end of this first stage, the caldera formed after the collapse of the old Gudda and the new Gudda edifice started to form. The post-caldera igneous phase constitutes the most important stage of the Boseti Volcanic Complex in terms of volume of magma erupted. The post-caldera activity started with the emplacement of pantelleritic lava flows which build up the Gudda volcanic edifice (Pleistocene-Holocene) and continued with intercalations of pomiceous deposits and lava flows, always with pantelleritic and comenditic compositions (as defined by Macdonald 1974). Almost simultaneously with the formation of Gudda, the Bariccia volcano (Pleistocene-Holocene) started to form in two episodes. Its formation involved two central episodes plus a lateral activity. The first episode is characterized by the emplacement of silicic products of trachytic composition followed by the emplacement of pyroclastic deposits of trachytic and rhyolitic composition with peralkaline affinity. The second episode is characterized by the emplacement of pantelleritic lava flows and pyroclastic deposits. The lateral activity of the Bariccia is represented by small lava flows of silicic composition with peralkaline affinity, localized on the northern sector (Brotzu et al. 1980).

Analytical techniques

This study on the Boseti Volcanic Complex presents forty-five new X-Ray Fluorescence major and trace element analyses, ICP-MS trace element analyses on eleven selected samples, about 1,000 new mineral and glass electron microprobe analyses on sixteen rocks and three bulk-rock Sr- isotopic data. Major- and trace-element concentrations have been obtained with X-ray Fluorescence Spectrometry (Panalytical AXIOS) at Centro Interdipartimentale di Strumentazioni per Analisi Geomineralogiche (CISAG), University of Naples. A subset of representative samples has been additionally analyzed with Inductively Coupled Plasma Mass Spectrometer at Actlabs (Canada; http://www.actlabs.com). Weight loss on ignition (LOI) has been determined with standard gravimetric procedures, after igniting the powder at ~900°C for ~5 h. Electron microprobe analyses have been performed with a Cameca Camebax SX50 at the IGG (Istituto di Geoscienze e

Georisorse, CNR, Padua) and with a similar instrument at IGAG (Istituto di Geologia Ambientale e Geoingegneria, CNR, Rome). A few more mineral analyses have been obtained at CISAG (Naples) using a JEOL JSM EDS microprobe. Sr isotopic analyses on three basalt samples have been obtained at the Osservatorio Vesuviano (INGV), Naples with a TRITON TI thermal ionization mass spectrometer, following the analytical techniques described in Di Renzo et al. (2007).

Rock nomenclature and petrography

The Boseti volcanic rocks have been classified using the TAS diagram (Le Bas et al. 1986; Fig. 2; Table 1). These rocks belong to the alkalic series, with Na_2O/K_2O ratios ranging between 0.9 and 6. A clear bimodal compositional distribution in terms of SiO_2 content is apparent from Fig. 2. Indeed, the samples cluster into two main groups: a basaltic-hawaiitic group (SiO_2 ~46–52 wt.%) and a trachytic-rhyolitic group (SiO_2 ~66–76 wt.%), with very scarce intermediate (mugearitic and benmoreitic) compositions. A few rocks are found in the range 52–66 wt.% SiO_2. Such a bimodal compositional distribution is typical of igneous rocks of almost all continental rifts, and in particular those of the MER (Trua et al. 1999; Peccerillo et al. 2003). The evolved samples have the Agpaitic Index [A.I. = molar $(Na_2O+K_2O)/Al_2O_3$] > 1 (up to 1.8). According to the FeO_t-Al_2O_3 diagram of Macdonald (1974) these samples are comendites and pantellerites. The CIPW norms of basic rocks range from ne-normative (maximum nepheline = 1.6 wt%) through hy-normative (maximum hypersthene = 16.7 wt%) to slightly qz-normative (maximum quartz = 2.1 wt%). The silicic rocks are rich in normative quartz (13.0–32.8%) and acmite (0.7–4.9%) (Table 1, Fig. 2).

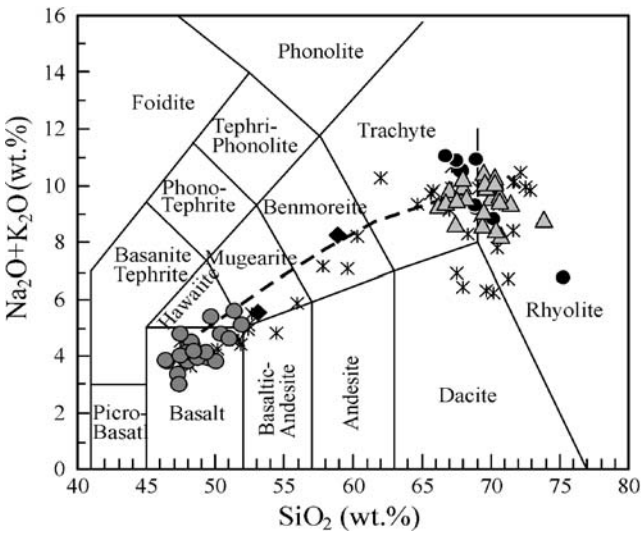

Fig. 2 Total Alkali vs. Silica (T.A.S.) classification diagram (Le Bas et al. 1986). Symbols: grey circles: basalts and hawaiites; black diamonds: mugearites and benmoreites; grey triangles: comendites and pantellerites. Asterisks are Gedemsa rocks (Peccerillo et al. 2003). The glass compositions in the evolved rocks are reported as black circles. The dashed line represents the MELTS fractional crystallization model

Petrography

The basalts are holocrystalline and mostly plagioclase-phyric, with subordinate olivine and clinopyroxene phenocrysts and micro-phenocrysts. In a few cases, euhedral to subhedral plagioclase phenocrysts are clustered in glomeroporphyric aggregates, occasionally associated with olivine and/or clinopyroxene phenocrysts or microphenocrysts. The groundmass phases are essentially the same as the phenocryst assemblage besides interstitial opaque minerals. Chromite inclusions have been found in olivine phenocrysts. Hawaiites are petrographically indistinguishable from the alkali basalts, showing the same phenocryst phases, whereas the groundmass assemblage has lower modal content of olivine.

Mugearites and benmoreites are aphyric to scarcely phyric with clinopyroxene and plagioclase phenocrysts set in a holocrystalline groundmass of clinopyroxene and Fe-Ti oxide or of essentially feldspar (benmoreite).

Trachytes and rhyolites are commonly glomeroporphyritic, with alkali feldspar, clinopyroxene and greenish olivine phenocrysts set in a glassy (often devitrified) groundmass. Alkali feldspar is the most common phase, both as euhedral to subhedral phenocryst and as groundmass phase. In a few cases, melt inclusions have been found within alkali feldspar phenocrysts. Olivine phenocrysts and micro-phenocrysts are commonly associated with alkali feldspar and/or clinopyroxene, often showing resorbed rims. The clinopyroxene phenocrysts and micro-phenocrysts are green, with anhedral to subhedral shape. Accessory phases are Fe-Ti oxides, aenigmatite and apatite. Fe-Ti oxides are always present principally associated with or included within clinopyroxene and olivine and rarely in alkali feldspar. Aenigmatite has been found both as phenocryst and groundmass phase, associated with clinopyroxene. Apatite has been found included in olivine phenocrysts of evolved rocks.

Mineral chemistry

Olivine

Olivine is observed in basic and evolved rocks as phenocryst and groundmass phase. The chemical composi-

Table 1 Major (wt.%), trace element (ppm) and $^{87}Sr/^{86}Sr$ isotope composition of Boseti rocks. A.I.= molar $(Na_2O+K_2O)/Al_2O_3$. The relative uncertainty of the Sr-isotope measurements is ±0.00001 (2σ)

	B458	B492	B501	B455	B463	B252	B209	B258	B465	B330	B212	B225	B497	B263	B494
SiO_2	46.45	46.54	48.70	47.51	49.32	47.31	47.98	49.43	48.98	47.81	48.27	47.37	48.45	50.03	50.46
TiO_2	2.19	1.93	1.96	2.17	2.14	2.57	2.21	1.82	2.01	1.61	2.49	1.69	2.82	2.53	2.59
Al_2O_3	15.78	16.20	14.45	16.82	15.73	15.29	14.51	16.24	17.08	17.03	14.89	17.13	15.26	14.26	16.37
Fe_2O_3t	12.11	11.61	10.66	11.96	10.64	11.25	13.08	10.47	12.11	10.40	13.11	10.46	13.88	11.03	12.11
MnO	0.18	0.18	0.17	0.18	0.17	0.17	0.19	0.15	0.19	0.16	0.19	0.16	0.19	0.18	0.18
MgO	7.63	7.37	7.10	7.06	6.75	6.28	6.10	5.94	5.80	5.74	5.62	5.49	5.03	4.57	4.21
CaO	10.00	10.10	11.75	10.31	9.92	10.11	9.22	9.59	9.23	10.86	8.82	12.32	10.54	10.33	9.00
Na_2O	3.03	2.96	3.00	3.22	3.09	2.53	2.87	2.95	3.29	3.13	3.45	2.25	3.40	2.78	3.48
K_2O	0.80	0.83	0.93	0.79	1.02	0.82	0.95	0.97	0.80	0.74	1.04	0.75	0.75	1.03	1.28
P_2O_5	0.43	0.41	0.37	0.47	0.43	0.32	0.39	0.33	0.27	0.33	0.37	0.27	0.28	0.26	0.38
LOI	1.42	1.87	0.91	−0.50	0.78	3.35	2.51	2.12	0.24	2.18	1.75	2.10	−0.61	3.01	−0.06
Sum	100.0	100.0	100.0	100.0	100.0	100.0	100.0	100.0	100.0	100.0	100.0	100.0	100.0	100.0	100.0
A.I.	0.37	0.36	0.41	0.37	0.39	0.33	0.40	0.36	0.37	0.35	0.46	0.26	0.42	0.40	0.43
Sc	26	24	30	27	24	26	28	22	22	30	29	32	32	28	25
V	319	241	287	293	256	310	317	283	279	284	372	293	371	336	293
Cr	318	352	416	209	209	204	37	17	39	90	20	60	38	25	35
Ni	89	75	59	80	54	97	31	39	19	30	23	40	21	44	23
Cu	50									40		130			
Zn	80									70		80			
Rb	17	12	15	17	15	17	22	20	14	16	25	12	12	26	22
Sr	478	409	384	482	430	975	399	426	482	391	424	691	394	400	433
Y	26	23	22	24	23	30	27	22	19	19	30	20	19	30	25
Zr	146	129	140	138	148	199	180	158	121	109	209	115	124	182	169
Nb	26	22	23	23	25	23	24	19	18	17	28	15	20	20	25
Ba	357	312	276	359	384	114	220	258	223	255	274	178	145	207	314
Cs	0.7														
La	25									18		20			
Ce	54	69	63	67	74	77	70	61	53	40	90	42	53	63	69
Pr	6.7									4.9		5.0			
Nd	28.2									20.8		20.9			
Sm	6.0									4.7		4.7			
Eu	2.3									1.7		1.6			
Gd	5.8									4.8		4.9			
Tb	0.9									0.8		0.8			
Dy	4.8									4.4		4.3			
Ho	0.9									0.8		0.8			
Er	2.4									2.3		2.2			
Tm	0.4									0.3		0.3			
Yb	2.1									2.0		1.9			
Lu	0.3									0.3		0.3			
Hf	3.4									2.9		2.9			
Ta	1.9									1.5		1.4			
Pb															
Th	1.9									1.8		1.9			
U	0.5									0.3		0.4			
$^{87}Sr/^{86}Sr$	0.704407									0.703930					

tion has a wide range from forsterite-rich (Fo_{85}) to pure fayalite (Fo_1; Table 2). Olivine phenocrysts of the basic products show essentially homogeneous composition; in a few cases, normal zoning (with Fo_{85-76} cores and Fo_{83-60} rims) is observed. Groundmass olivine in the basic rocks is more Fe-rich (Fo_{65-36}). Olivine in pantellerites and comendites has the lowest forsterite contents (Fo_{10-1}). Minor elements such as Mn and Ca decrease towards the most fayalite-rich types (from 5.71 wt.% to 4 wt.% MnO; from 0.8 wt.% to 0.2 wt.% CaO).

Clinopyroxene

Clinopyroxene of basalts and hawaiites is mostly augite, and typically has normal zoning with Fe-rich (and MgO-poor) rims compared to the cores. The TiO_2 contents

Table 1 (continued)

	B378	B495	B503	B270	B247	B332	B268	B450	B375	B269	B262	B175	B302	B345	B306
SiO_2	47.96	51.04	51.95	47.50	53.08	49.67	51.37	58.86	67.48	73.89	70.75	70.04	71.42	69.42	66.70
TiO_2	2.27	2.20	1.90	3.02	2.67	2.73	2.18	1.34	0.58	0.39	0.49	0.45	0.35	0.54	0.56
Al_2O_3	18.24	15.52	17.27	14.11	14.73	15.95	16.57	15.40	9.52	9.65	10.97	12.36	11.45	8.41	12.10
Fe_2O_3t	11.73	11.91	10.47	14.28	9.09	12.53	11.22	9.94	9.82	5.39	5.52	5.95	5.64	9.55	7.98
MnO	0.18	0.22	0.16	0.24	0.14	0.21	0.20	0.36	0.41	0.20	0.15	0.27	0.20	0.29	0.35
MgO	4.21	4.19	4.06	3.95	3.89	3.76	3.37	1.11	0.53	0.48	0.38	0.16	0.14	0.14	0.14
CaO	10.72	8.61	8.77	8.89	7.02	8.44	8.83	3.82	0.90	0.31	0.18	0.66	0.55	0.54	1.55
Na_2O	3.53	3.41	3.81	3.81	3.81	4.26	4.23	6.20	4.57	4.28	3.94	5.67	5.08	4.35	5.76
K_2O	0.59	1.20	1.27	0.98	1.72	1.10	1.34	2.06	4.06	4.53	4.29	3.89	4.29	4.27	3.64
P_2O_5	0.36	0.30	0.56	0.70	0.70	0.58	0.81	0.37	0.03	0.03	0.03	0.03	0.01	0.02	0.06
LOI	0.20	1.39	−0.22	2.53	3.16	0.76	−0.11	0.56	2.10	0.85	3.29	0.51	0.87	2.48	1.17
Sum	100.0	100.0	100.0	100.0	100.0	100.0	100.0	100.0	100.0	100.0	100.0	100.0	100.0	100.0	100.0
A.I.	0.35	0.45	0.44	0.52	0.55	0.51	0.51	0.81	1.25	1.24	1.01	1.10	1.13	1.40	1.11
Sc	26	25	23	31	19	28	32	18	2	7	9	6	2	1	6
V	374	303	265	390	252	329	310	31	19		9	15			39
Cr	78	13	16	67			15								
Ni	39	15	10	32	3	7	18	8	4	2	6	3	5	3	2
Cu						20	30								
Zn					120	120	100	120						290	
Rb	8	12	14	13	39	11	19	26	59	115	111	79	88	116	65
Sr	462	437	532	448	535	404	407	324	25	74	7	12	11	12	25
Y	19	25	27	41	43	26	32	43	73	105	78	64	95	144	61
Zr	89	155	162	167	273	146	169	236	474	761	806	590	721	1007	456
Nb	15	21	24	24	34	24	25	42	89	103	110	106	119	179	84
Ba	122	495	409	358	696	381	600	867	676	38	467	821	603	104	1312
Cs								0.5						1.5	
La					46	28	33	47						130	
Ce	63	73	65	101	95	61	71	99	136	202	170	156	192	260	120
Pr					12.2	7.7	9.2	12.2						31.0	
Nd					51.0	32.9	40.6	50.6						119.0	
Sm					10.9	7.7	8.9	10.8						26.0	
Eu					3.7	2.9	3.6	4.7						5.1	
Gd					10.9	7.7	8.9	10.5						25.6	
Tb					1.7	1.2	1.4	1.7						4.5	
Dy					8.9	6.6	7.6	9.4						26.4	
Ho					1.6	1.2	1.4	1.8						5.2	
Er					4.4	3.4	3.8	5.1						15.6	
Tm					0.6	0.5	0.5	0.7						2.4	
Yb					3.6	2.9	3.3	4.5						14.7	
Lu					0.5	0.4	0.5	0.7						2.2	
Hf					7.2	4.8	4.7	7.0						25.8	
Ta					2.8	2.4	2.3	3.6						12.6	
Pb					7.0			8.0						23.0	
Th					5.1	2.3	2.3	5.1						18.2	
U					1.2	0.7	0.3	1.2						4.4	
$^{87}Sr/^{86}Sr$							0.704181								

reach values as high as 3.5 wt.%, and Al_2O_3 values as high as 5 wt.% (Table 2; Fig. 3). Clinopyroxene of intermediate rocks is characterized by a composition similar to groundmass clinopyroxene of the basic rocks (Table 2; Fig. 3). Clinopyroxene of pantellerites and comendites is Fe-augite (hedenbergite) or, more rarely, aegirine-augite, and is characterized by low Ti and high Fe, Mn and Na compared to clinopyroxene of the basalts and hawaiites. A few crystals show relatively wide variation in Na between rim and core with aegirine-augite rims and Fe-augite cores. Na_2O reaches values as high as 5 wt.%, but is generally lower than 3 wt.%. The relatively wide range of Al and Ti content in the basic rocks reflects the substitution: $(Mg, Fe)^{VI} + 2\ Si^{IV} = Ti^{VI} + 2\ Al^{IV}$. The small range of Na in clinopyroxene of basic and intermediate products reflects the minor importance of this element in the

B305	B244	B301	B307	B355	B319	B303	B357	B322	B354	B350	B337	B341	B343	B373
68.26	70.40	70.67	66.16	67.02	67.56	69.46	70.63	68.01	69.66	69.45	70.26	69.59	70.29	67.97
0.42	0.49	0.30	0.55	0.61	0.49	0.36	0.38	0.45	0.55	0.57	0.53	0.55	0.54	0.56
12.52	9.38	11.78	12.54	11.55	12.33	10.94	12.70	11.88	7.60	8.56	8.08	7.81	7.85	10.08
6.79	7.91	5.55	7.93	8.98	7.29	5.83	5.20	6.06	10.18	10.05	10.02	9.96	9.81	9.39
0.29	0.14	0.20	0.35	0.36	0.31	0.20	0.21	0.26	0.30	0.30	0.30	0.30	0.29	0.34
0.13	0.13	0.12	0.11	0.08	0.05	0.05	0.02	0.00	0.00	0.00	0.00	0.00	0.00	0.00
1.02	0.26	0.60	1.31	0.35	1.06	1.28	0.64	0.90	0.42	0.38	0.35	0.35	0.35	0.60
5.52	4.12	5.01	5.83	6.02	5.67	4.95	5.75	5.38	5.70	6.24	6.08	5.86	5.88	6.05
4.05	4.31	4.42	3.47	3.84	3.81	4.14	3.89	4.61	4.25	4.23	4.20	4.26	4.23	4.23
0.03	0.03	0.01	0.05	0.04	0.06	0.01	0.02	0.03	0.02	0.02	0.02	0.02	0.02	0.04
0.97	2.84	1.34	1.69	1.14	1.35	2.76	0.54	2.41	1.32	0.21	0.15	1.31	0.73	0.75
100.0	100.0	100.0	100.0	100.0	100.0	100.0	100.0	100.0	100.0	100.0	100.0	100.0	100.0	100.0
1.07	1.22	1.11	1.06	1.22	1.09	1.15	1.08	1.16	1.84	1.73	1.80	1.82	1.82	1.44
2		1	10	4	3	5	4		2	1		1	2	
48		7	48	35	43	9	6							16
										10				
8	4	7	7	6	4	7	1		3	21	8	3	2	1
							170		270			290		
75	134	109	61	50	68	110	88	55	148	121	157	136	131	53
24	3	17	35	25	23	14	13	4	0	9	1	0	0	3
80	103	102	72	62	73	106	84	54	161	140	170	151	148	62
545	976	777	496	424	504	809	675	368	1182	927	1207	1082	1058	437
97	148	129	92	73	91	134	116	71	211	165	215	194	190	77
1162	93	603	1221	1093	1011	545	603		109	103	97	95	91	630
							0.8		2.1			2.0		
							83		149			140		
159	186	207	144	123	139	217	168		296	294	322	284	299	138
							19.1		35.1			33.0		
							70.7		135.0			126.0		
							14.8		29.1			28.2		
							2.8		5.7			5.6		
							14.3		28.4			27.1		
							2.5		5.1			4.8		
							15.1		30.3			28.8		
							2.9		5.8			5.6		
							9.1		17.3			16.7		
							1.4		2.7			2.5		
							9.1		16.6			16.2		
							1.4		2.4			2.3		
							16.4		30.3			27.8		
							7.6		14.4			13.8		
							18.0		21.0			27.0		
							12.4		20.8			19.4		
							2.7		5.4			5.1		

augite structure while it becomes more important for the evolved rocks with the substitution: $(Fe^{2+}+Mg)^{VI} + (Ca^{2+})^{M2} = (Fe^{3+})^{VI} + (Na^{+})^{M2}$.

Feldspar

Plagioclase phenocrysts of the basic rocks have bytownite cores (An_{86-68}-Ab_{43-13}-Or_{2-0}) and bytownite-labradorite rims (An_{86-48}-Ab_{48-13}-Or_{2-0}), while groundmass plagioclase varies from bytownite to andesine (An_{70-38}-Ab_{68-44}-Or_{11-1}). The intermediate rocks have plagioclase phenocrysts ranging from labradorite to oligoclase (An_{21-55}-Ab_{42-72}-Or_{1-9}). The evolved rocks, being peralkaline, lack plagioclase both as a phenocryst and as groundmass phase; they are characterized by anorthoclase and, subordinately, sanidine phenocrysts (An_{4-0}-Ab_{82-52}-Or_{47-15}) (Table 3; Fig. 4).

Table 2 Representative electron microprobe analyses of clinopyroxene and olivine from Boseti Volcanic Complex

Sample		SiO_2	TiO_2	Al_2O_3	FeO	MnO	MgO	CaO	Na_2O	Cr_2O_3	Sum	Wo	Fs	En
pyroxene														
B330	c	50.27	1.48	3.05	9.51	0.22	13.47	20.82	0.46	0.00	99.3	44.1	16.1	39.7
B330	r	50.90	0.97	0.88	15.30	0.48	10.26	19.91	0.59	0.05	99.3	42.8	26.5	30.7
B225	c	51.41	0.96	3.14	7.11	0.29	16.51	20.43	0.24	0.11	100.2	41.5	11.7	46.7
B225	r	49.31	1.24	5.17	6.79	0.12	14.58	22.48	0.27	0.21	100.2	46.7	11.2	42.1
B492	c	46.51	3.34	4.72	10.84	0.19	11.70	20.80	0.54	0.03	98.7	45.5	18.8	35.6
B450	c	51.40	0.66	1.32	14.38	1.03	11.32	20.27	0.42	0.00	100.8	42.2	25.1	32.8
B450	r	51.36	0.82	1.59	13.80	0.88	11.96	19.95	0.41	0.04	100.8	41.5	23.9	34.6
B345	c	48.38	0.40	0.12	25.47	1.78	3.43	18.05	1.84	0.00	99.5	40.9	48.3	10.8
B345	r	47.64	0.48	0.16	30.22	1.59	0.14	18.33	1.44	0.00	100	42.3	57.3	0.5
B357	c	48.53	0.68	0.64	24.44	2.10	4.04	19.06	0.59	0.05	100.1	42.0	45.7	12.4
B322	gm	49.22	1.05	0.39	28.13	2.00	0.70	17.17	1.05	0.12	99.8	41.2	56.5	2.3
B350	gm	47.28	1.22	0.24	28.92	1.40	0.16	15.68	2.57	0.00	97.5	39.6	59.8	0.6
B375	r	51.43	0.76	0.17	28.91	1.08	0.16	13.88	5.20	0.03	101.6	37.0	62.4	0.6
olivine														Fo
B330	c	40.36			16.17	0.26	44.32	0.27			101.4			83.0
B330	r	35.92			36.64	0.73	26.79	0.41			100.5			56.6
B492	c	40.83			14.50	0.23	45.30	0.24		0.06	101.2			84.8
B492	c	39.75			15.20	0.17	43.86	0.32		0.05	99.4			83.7
B492	c	40.54			15.41	0.15	44.70	0.25		0.08	101.1			83.8
B268	gm	32.94			47.51	1.17	17.57	0.47			99.7			39.7
B175	c	29.98			61.72	5.60	3.50	0.52		0.01	101.3			9.2
B175	r	30.06			61.81	5.71	3.22	0.55			101.3			8.5
B355	c	29.81			65.65	5.14	0.43	0.37			101.4			1.1
B303	r	27.87			63.06	4.62	0.11	0.27			95.9			0.3

Forsterite = 100 $Mg/(Mg+Fe^{2+})$; Wo (wollastonite), Fs (ferrosilite), En (enstatite) in mol.%

c core, *r* rim, *gm* groundmass

Oxides

Cr-rich spinels, Ti-magnetite and ilmenite have been found in the Boseti lavas. Cr-rich spinel inclusions with Cr_2O_3 up to 36 wt.% and Cr#[$Cr\# = \text{molar Cr} * 100/(Cr + Al)$] ranging from 16 to 49 have been found as inclusions in olivine of alkali basalts (Table 4). The Ti-magnetite has variable ulvöspinel content (47–86 mol %; 16.7–29.3 wt.% TiO_2). MnO ranges from 0.31 wt.% to 2.68 wt.% and the Al_2O_3 content is generally low (0.23–2.30 wt.%). Rare ilmenite crystals have been found. They have 74–98 mol.% ilmenite, and relatively high MnO (>2 wt.%) (Table 4). Geothermometric and fO_2 estimates according to ilmenite-magnetite calibrations (Lepage 2003) show a large range in temperature (from ~840°C to ~1,240°C). The fO_2 values mostly correspond to those of the QFM buffer.

Aenigmatite and apatite

Aenigmatite and apatite are minor or accessory phases in the Boseti rocks (Table 5). Aenigmatite is a phenocryst and/or groundmass phase in comendites and pantellerites. It is not present in all the Boseti evolved rocks, and is always associated with clinopyroxene, K-feldspar, fayalite and opaque minerals. This mineral has high TiO_2 (7.50–8.94 wt.%) and Na_2O (5.80–7.54 wt.%) contents. Apatite is found in both groundmass of the basic rocks and as inclusions in fayalite phenocrysts in the evolved rocks.

Glass

The original glassy matrix of comendites and pantellerites suffered devitrification processes at low temperature. Fresh glass has been analyzed defocusing the electron beam to a spot area of 20 μm in diameter. These glasses are trachytic to rhyolitic (Fig. 2; Table 5), and are strongly peralkaline (A.I.=1.23–1.92), similar to the bulk rock compositions (Fig. 2).

Geochemistry

Major and trace element contents are plotted vs. SiO_2 content in Fig. 5. The gap in SiO_2 appears evident. The mafic rocks have CaO, MgO, Cr, Ni, V, Sc decreasing with increasing silica, whereas TiO_2, Fe_2O_{3t}, Na_2O and Sr show scatter, and K_2O, Rb, Zr, Y, Nb increase with silica. A few basic samples showing anomalously high Sr contents, are characterized by the presence of excess plagioclase phenocrysts. The silicic rocks have decreasing Fe_2O_{3t}, TiO_2, CaO, Al_2O_3 and Na_2O contents with increasing silica. The Sr content is very low, Ba markedly decreases and elements

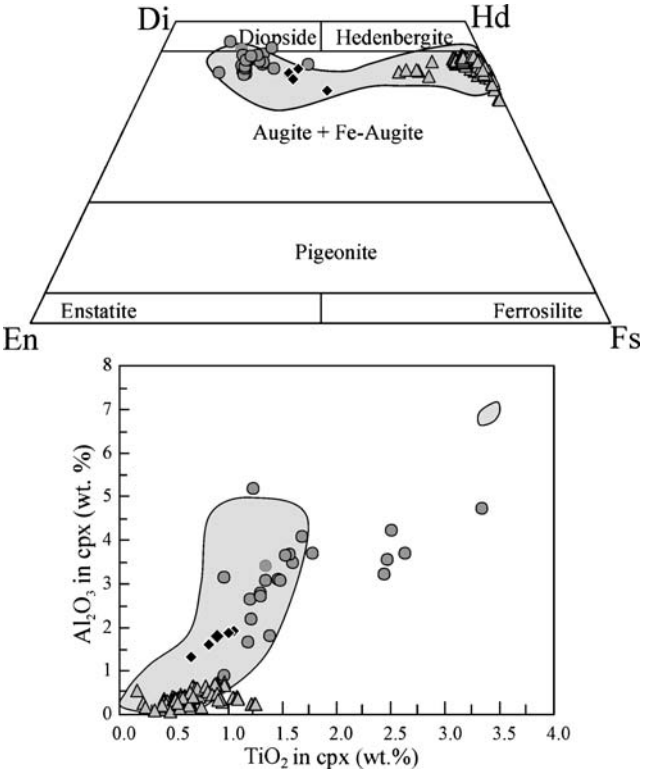

Fig. 3 Classification diagram for the Boseti clinopyroxenes, and Al_2O_3-TiO_2 diagram (wt.%) for the same compositions. Symbols are the same of Fig. 2. The areas report the field of clinopyroxene compositions of Brotzu et al. (1974) and Carbonin et al. (1991)

such as Rb, Y, Zr, Nb markedly increase with increasing silica, reaching high abundances in the pantellerites (Fig. 5). Overall, the Boseti rocks display major element variation trends similar to those from the Gedemsa volcano, located not far from Boseti (Fig. 5).

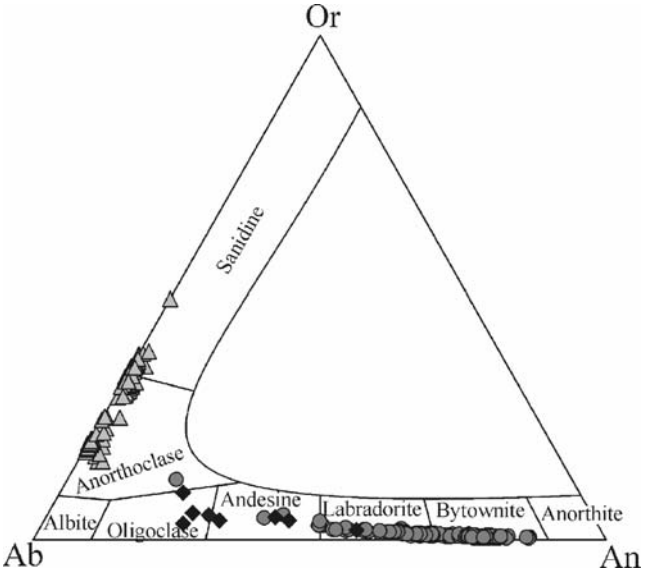

Fig. 4 Composition of Boseti feldspars in the anorthite-albite-orthoclase diagram (mol.%). Symbols as in Fig. 2

Incompatible-incompatible element diagrams (Rb, Y and Nb vs. Zr; Fig. 5) show broadly linear trends. This feature is found in other EARS volcanic complexes (Barberi et al. 1975; Trua et al. 1999; Peccerillo et al. 2003, 2007). Chondrite-normalized REE patterns of the Boseti basalts show a small Eu positive anomaly (Fig. 5) and enrichment of LREE over HREE (La/Yb_N=7–14, where the subscript N means chondrite-normalized). The evolved rocks show patterns with lower LREE/HREE ratios compared to the basic types (La/Yb_N=5.8–7.1). Europium negative anomalies are present in the silicic rocks (Eu/Eu*=0.58–0.62, where Eu is normalized Eu and Eu* is Eu interpolated between normalized Sm and Gd).

Table 3 Representative electron microprobe analyses of feldspar from Boseti Volcanic Complex

Sample		SiO_2	Al_2O_3	FeO_t	MgO	CaO	Na_2O	K_2O	sum	Ab	An	Or
B225	c	46.72	33.11	0.52	0.18	17.96	1.49	0.06	100.0	13.0	86.6	0.3
B225	r	51.68	29.49	0.58	0.05	12.93	3.92	0.38	99.0	34.6	63.1	2.2
B492	c	50.72	30.68	0.54	0.18	14.73	3.05	0.14	100.0	27.1	72.1	0.8
B492	r	54.59	28.13	0.59	0.14	11.32	5.19	0.41	100.4	44.3	53.4	2.3
B332	c	49.22	32.94	0.56	0.07	16.28	2.31	0.11	101.5	20.3	79.1	0.6
B332	r	53.17	30.15	0.72	0.10	12.88	4.12	0.24	101.4	36.1	62.4	1.4
B330	gm	56.22	27.08	0.55	0.09	10.32	5.70	0.51	100.5	48.6	48.6	2.8
B450	gm	63.02	21.95	0.78	0.05	4.49	8.01	1.64	99.9	69.2	21.5	9.3
B450	gm	63.07	23.02	0.29	0.03	5.14	8.32	0.54	100.4	72.2	24.7	3.1
B175	c	66.19	18.58	0.47	0.08	0.71	9.14	2.65	97.8	81.1	3.5	15.5
B175	r	67.11	18.59	0.36	0.01	0.53	9.11	2.86	98.6	80.7	2.6	16.6
B322	c	67.78	18.40	0.43	0.05	0.16	7.22	5.81	99.9	64.9	0.8	34.3
B355	c	68.22	18.88	0.51	0.00	0.05	9.48	3.41	100.6	80.7	0.3	19.1
B350	c	68.99	18.46	0.88	0.01	0.05	7.65	5.62	101.7	67.2	0.3	32.5
B350	r	67.88	18.10	0.85	0.11	0.13	7.89	5.25	100.2	69.1	0.6	30.3
B350	c	68.16	18.42	1.01	0.05	0.01	7.78	5.76	101.2	67.2	0.0	32.7

An (Anorthite), Ab (Albite) and Or (Orthoclase) in mol.%

c core, *r* rim, *gm* groundmass

Table 4 Representative electron microprobe analyses of oxides from Boseti Volcanic Complex. Ulvöspinel and ilmenite in mol%

Sample		TiO_2	Al_2O_3	FeO	MnO	MgO	Cr_2O_3	NiO	V_2O_5	Sum	Mg#	Cr#
chromite												
B492	in olivine	0.78	27.70	23.46	0.37	14.13	32.00	0.24	0.23	98.9	63	44
B492	in olivine	0.34	25.12	22.38	0.27	13.34	36.06	0.00	0.13	97.6	61	49
B492	in olivine	0.59	26.61	21.49	0.39	15.95	32.38	0.00	0.35	97.8	72	45
B492	in olivine	3.88	37.13	32.30	0.13	13.98	11.86	0.62	0.06	100.0	56	18
B492	in olivine	1.71	31.22	32.28	0.28	11.64	20.89	0.15	0.37	98.5	51	31
magnetite												Ulvöspinel
B175	c	22.19	0.28	73.30	2.40	0.12	0.01			100.9		62%
B175	c	22.16	0.25	73.89	2.19	0.09	0.00			101.3		62%
B492	gm	25.95	1.19	60.86	0.54	1.11	0.00			90.8		79%
B258	c	16.45	1.77	75.42	0.31	0.87	0.12			98.4		47%
B258	c	17.43	1.66	74.94	0.40	0.87	0.04			98.6		50%
B330	gm	25.36	1.46	64.94	0.47	1.13	0.00			94.9		74%
B330	gm	29.33	0.76	61.81	0.62	1.29	0.06			94.7		86%
ilmenite												
B345	c	52.02	0.02	46.41	2.17	0.00	0.02			100.8		98%
B303	gm	45.73	0.14	44.44	2.36	0.00	0.00			93.3		93%
B303	gm	46.89	0.20	43.10	2.83	0.00	0.00			93.4		95%

$Mg\# = Mg * 100/(Mg + Fe_{2+})$; $Cr\# = Cr * 100/(Cr + Al)$; ulvöspinel and ilmenite in mol.%

c core, *gm* groundmass

Primitive mantle-normalized incompatible element patterns for the basalts are reported in Fig. 6. The Boseti basalts show incompatible element patterns intermediate between the average composition of LT- (Low-Ti) and HT- (High-Ti) type basalts of the Ethiopian Plateau (Pik et al. 1998, 1999; Kieffer et al. 2004). The incompatible trace element pattern of the Boseti basalts matches the composition of other MER basalts fairly well (Fig. 6).

Sr isotopes

Three Boseti basalts have been analyzed for Sr isotopic ratios (Table 1). The $^{87}Sr/^{86}Sr$ ratios range from 0.7039 to 0.7044. These data plot well within the field of other MER basalts (Peccerillo et al. 2003; Furman et al. 2006b and references therein)(Fig. 7).

Discussion

Origin of the basic rocks

The Ethiopian continental flood basalts have been the object of several studies (Betton and Civetta 1984; Hart et al. 1989; Vidal et al. 1991; Pik et al. 1998, 1999; Kieffer et al. 2004). Many models have been developed to explain the huge volume of magma produced, the composition of the basic rocks and their relation with

Table 5 Representative electron microprobe analyses of aenigmatite, apatite and glass of Boseti rocks

		SiO_2	TiO_2	Al_2O_3	FeO	MnO	MgO	CaO	Na_2O	K_2O	Sum		
B350	aenig	39.33	7.74	1.33	39.69	1.15	0.09	1.02	5.80	0.32	96.5		
B350	aenig	39.88	8.07	0.80	41.59	1.20	0.00	0.90	6.37	0.32	99.1		
B375	aenig	39.91	8.37	0.26	39.11	1.53	0.04	0.23	6.97	0.17	96.6		
B375	aenig	43.60	7.50	0.76	39.12	1.49	0.04	0.40	6.57	0.24	99.7		
B355	aenig	41.79	8.94	0.29	42.27	1.23	0.12	0.21	7.48	0.02	102.4		
B355	aenig	41.13	8.52	0.45	41.15	1.16	0.21	0.48	6.88	0.01	100.0		
Sample		FeO	MnO	CaO	Na_2O	K_2O	P_2O_5	F	Sum				
B322	ap	2.50	0.08	50.32	0.16	0.23	39.99	3.22	96.5				
B322	ap	2.73	0.35	49.50	0.17	0.08	41.27	4.43	98.5				
B303	ap	3.00	0.02	48.11	0.42	0.11	38.51	4.53	94.7				
		SiO_2	TiO_2	Al_2O_3	FeO	MnO	MgO	CaO	Na_2O	K_2O	SrO	BaO	Sum
B354-2	glass	67.89	0.51	8.55	8.68	0.34	0.02	0.48	6.05	4.47		0.06	97.0
B354	glass	68.99	0.58	8.46	8.47	0.32	0.00	0.40	6.53	4.40			98.1
B322	glass	68.00	1.05	3.98	13.34	0.71	0.09	1.69	4.26	3.70	0.88	0.02	97.7
B350	glass	69.53	0.85	4.91	11.69	0.23	0.17	0.67	6.08	4.19	0.60	0.28	99.2
B375	glass	65.10	0.45	2.40	16.09	1.56	0.05	0.70	6.53	3.30	0.40	0.22	96.8

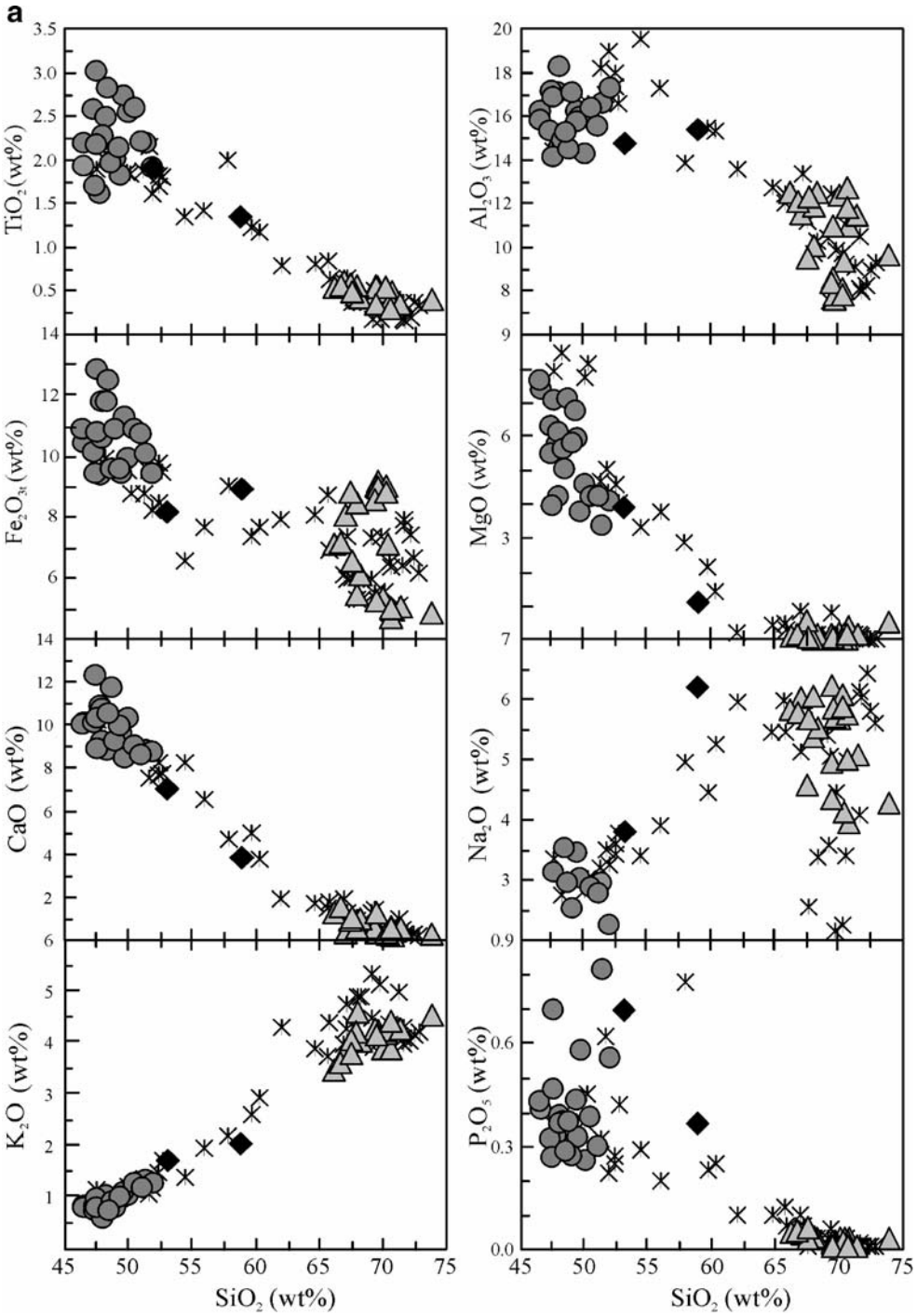

Fig. 5 Major and trace element diagrams (including REE chondrite-normalized patterns). Symbols are the same of Fig. 2. Asterisks are Gedemsa rocks (Peccerillo et al. 2003). Chondrite values used for nomalization are those of Boynton (1984). Bulk partition coefficients used in the diagrams with Zr as abscissa are: D_{Zr}=0.06; D_{Rb}=0.1; D_{Y}=0.16; D_{Nb}=0. The value of residual liquid fraction (in mass%) is reported close to the tick marks

the differentiated peralkaline rocks A two-source mixing model has been proposed to explain the geochemical variability of the Ethiopian basalts. In particular, the involvement of both depleted asthenosphere and enriched sub-continental lithospheric mantle sources has been invoked by several researchers (Betton and Civetta 1984). The Afar volcanism has been interpreted as the result of mixing between melts of old mantle lithosphere and HIMU-type mantle plume sources (Vidal et al. 1991). Three potential sources have been considered for the Gulf of Aden basalts: a hybrid EM1-EM2 mantle source, a HIMU-like mantle plume and a depleted asthenosphere.

The composition of the Boseti basalts is almost identical with that of other rift floor basalts in terms of geochemistry and petrography. The relatively low $^{87}Sr/^{86}Sr$ (<0.7044) of the three analyzed basalts seem to exclude a major role for upper crustal contamination processes.

Fig. 5 (continued)

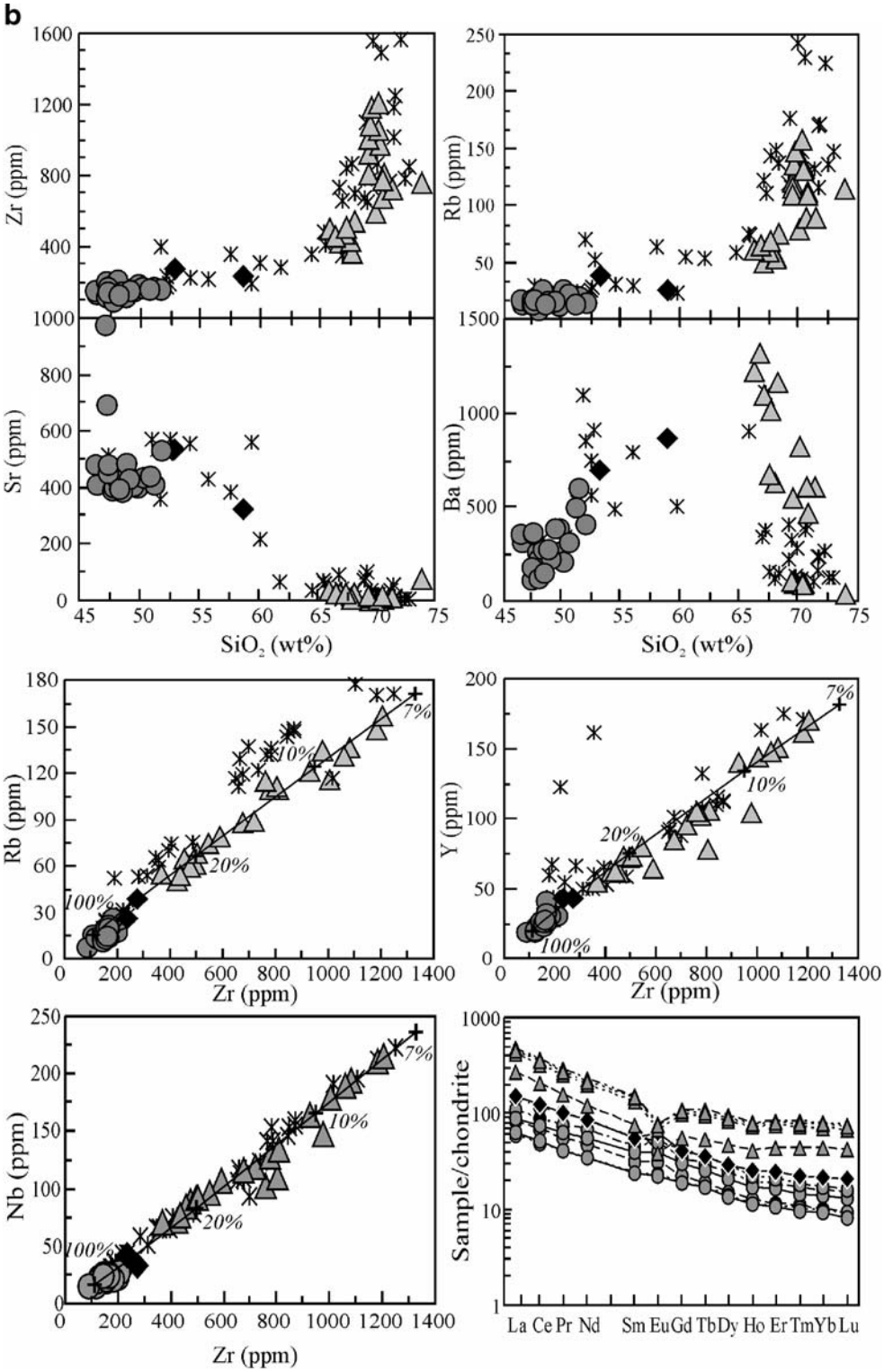

Origin of the evolved rocks

The origin and geodynamic significance of peralkaline magmatism is one of the most intriguing tasks of igneous petrology. From a tectonic point of view, peralkaline rocks are commonly emplaced in oceanic intraplate (e.g., Ascension and Azores islands in the Atlantic Ocean) or continental rift (e.g., EAR). However, the common interpretation that comendites and pantellerites are never related to subduction settings (e.g., Maniar and Piccoli

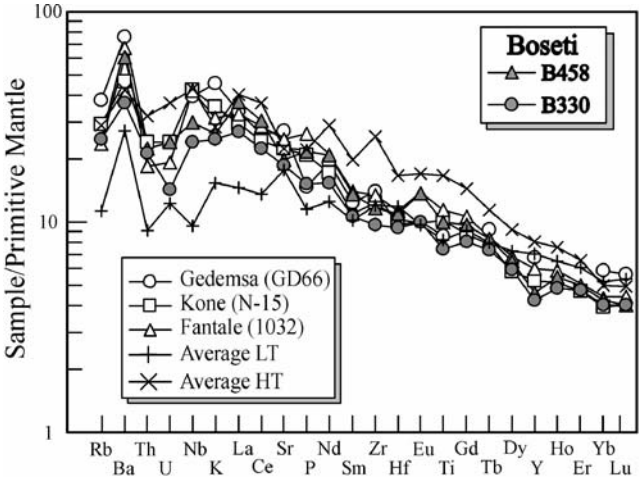

Fig. 6 Primitive mantle normalized trace element patterns of Boseti basalts (normalizing values after Sun and McDonough 1989). The patterns of mafic samples from Gedemsa, Kone and Fantale are also reported (data from Furman et al. 2006a; Peccerillo et al. 2003). The average low-Ti and high-Ti Ethiopian flood basalts are from Kieffer et al. (2004)

1989) is not valid, since subduction-related silicic peralkaline rocks have been found elsewhere (e.g. in Sardinia, Italy; Morra et al. 1994; Lustrino et al. 2004).

During the last 40 years, many researchers have investigated such compositions, particularly in the EARS, obtaining often contrasting results. Two are the main hypotheses proposed in the literature to explain the origin of peralkaline igneous activity associated with continental rifting stages. The first model is based on prolonged fractional crystallization of a transitional basaltic parental melt, possibly involving a minor role for crustal contamination (Barberi et al. 1975; Geist et al. 1995; Mungall and Martin 1995; Civetta et al. 1998; Trua et al. 1999; Peccerillo et al. 2003, 2007). The alternative hypothesis considers the peralkaline rocks as originated by partial melting of local crust triggered by alkali-bearing volatiles (Macdonald et al. 1987; Black et al. 1997; Scaillet and Macdonald 2001, and references therein). Fractional crystallization processes can explain some geochemical characteristics of the peralkaline melts but fail to explain the lack of rocks with intermediate composition (the so-called Daly Gap) and the high volume of evolved rocks (Peccerillo et al. 2003). Worth noting is that the Daly Gap may be more apparent than real. The non-eruption of intermediate magma can be related to its high viscosity, preventing it from erupting. More silicic magmas (pantellerites and comendites) have still higher viscosities, but they are associated to much lower density. This feature and the higher volatile content of silicic magma help to drive them out from the magma reservoirs.

An important role in the formation of peralkaline magmas is played by clinopyroxene and other Na-bearing phases such as aenigmatite (cf. White et al. 2005). Experimental studies (Bailey and Cooper 1978; Scaillet and Macdonald 2001) show that temperature, H_2O activity, melt composition and fO_2 affect clinopyroxene stability and composition. Low fO_2 destabilizes Na-rich clinopyroxene that transforms into a fayalite-ilmenite ± fluorite assemblage. Moreover, anhydrous conditions inhibit aegirine and Na-rich amphibole crystallization. However, high fO_2 expands the stability field of these two phases and inhibits olivine and ilmenite crystallization. In particular, fO_2 values below QFM buffer at temperatures below 800°C favour the development of peralkaline liquids without the appearance of aegirine or sodic amphibole as liquidus phases. The disappearance of these Na-rich phases leads to an increase of the Na_2O content in the residual liquid, possibly evolving towards peralkaline compositions.

Aenigmatite is divided into a Ti-free aenigmatite and Ti-bearing aenigmatite (Lindsley 1971; Scaillet and Macdonald 2001, and references therein). Titanium-free aenigmatite is unstable at pressures above 0.9 kb, while Ti-bearing aenigmatite was synthesized at 1 kb. Most likely, its stability is pressure- and fO_2-dependent, being stable at relatively low fO_2. Ti-free aenigmatite is unstable at fO_2 above WM buffer whereas the Ti-bearing variety is stable between NNO and QFM buffers. Relatively reduced conditions of mantle sources are evidenced by Fe-Ti oxide thermometry and oxygen barometry, indicating values close to QFM buffer. The occurrence of aenigmatite is probably the main reason for the lack of very aegirine-rich clinopyroxenes in the Boseti silicic rocks.

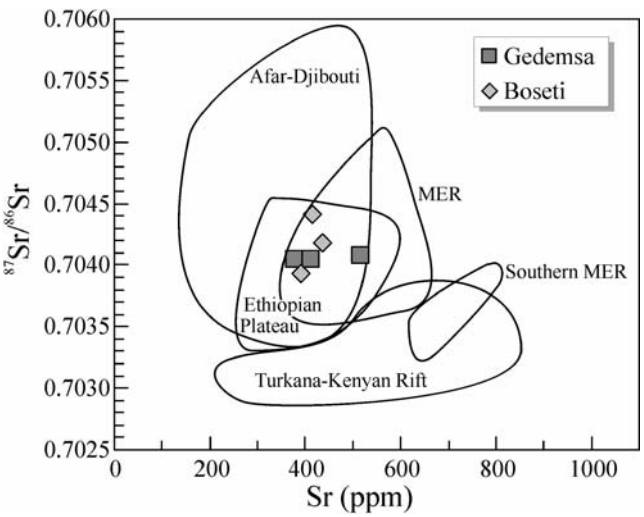

Fig. 7 Sr vs. $^{87}Sr/^{86}Sr$ diagram for the basalts of Boseti Volcanic Complex. **a**–**d** (Afar-Djibouti; Barberi et al. 1980; Deniel et al. 1994), MER (Main Ethiopian Rift; Furman et al. 2006b), EP (Ethiopian Plateau; Pik et al. 1999; Kieffer et al. 2004), T-KR (Turkana-Kenyan Rift; Furman et al. 2004, 2006a), SMER (Southern Main Ethiopian Rift; George and Rogers 1999). The Gedemsa basalts are from Peccerillo et al. (2003)

Table 6 Results of mass balance calculations for the transition from mafic to evolved Boseti rocks

Sample	From: B492	To: B450	Chemical compositions				%rem. Solid	Res^2
			Ol	Cpx	Plag	Op		
SiO_2	48.45	59.19	40.66	47.15	50.71			0.03
TiO_2	1.94	1.35	0.00	3.38	0.00	24.91		0.11
Al_2O_3	16.04	15.48	0.00	4.78	30.67	1.46		0.01
FeO	11.78	10.00	23.44	10.99	0.54	71.73	−71.0	0.00
MnO	0.17	0.36	0.35	0.19	0.00	0.64		0.00
MgO	7.03	1.11	34.88	11.86	0.18	1.24		0.01
CaO	10.16	3.84	0.76	21.09	14.72	0.00		0.00
Na_2O	3.15	6.23	0.00	0.54	3.05	0.00		0.03
K_2O	0.83	2.07	0.00	0.00	0.14	0.01		0.03
P_2O_5	0.44	0.37						0.11
Fract. Solid wt.%			13.0	18.0	34.9	5.1	$\sum R^2$	**0.33**
Sample	From: B450	To: B355	Chemical compositions				%rem. Solid	Res^2
			Cpx	Plag	Op			
SiO_2	59.19	67.80	49.61	61.06				0.03
TiO_2	1.35	0.61	1.05	0.00	20.09			0.05
Al_2O_3	15.48	11.68	1.91	23.55	1.65			0.01
FeO	10.00	9.09	17.81	0.69	75.88		−57.4	0.01
MnO	0.36	0.37	1.23	0.00	0.82			0.00
MgO	1.11	0.08	9.91	0.07	1.56			0.05
CaO	3.84	0.36	18.00	5.96	0.00			0.06
Na_2O	6.23	6.09	0.48	7.79	0.00			0.03
K2O	2.07	3.89	0.00	0.87	0.00			0.00
P_2O_5	0.37	0.04						0.12
Fract. Solid wt.%			7.3	44.0	6.1		$\sum R^2$	**0.37**
Sample	From: B355	To: B302	Chemical compositions				%rem. Solid	Res^2
			Ol	Cpx	alkalifeldspar	Op		
SiO_2	67.80	72.05	29.84	48.46	68.31			0.00
TiO_2	0.61	0.35	0.00	0.46	0.00	22.57		0.00
Al_2O_3	11.68	11.55	0.00	0.20	18.74	0.28		0.14
FeO	9.09	5.69	64.69	28.60	0.38	74.56	−25.68	0.00
MnO	0.37	0.20	4.73	1.70	0.00	2.44		0.01
MgO	0.08	0.14	0.43	0.77	0.00	0.12		0.00
CaO	0.36	0.55	0.31	18.40	0.07	0.00		0.01
Na_2O	6.09	5.12	0.00	1.42	9.17	0.00		0.35
K_2O	3.89	4.33	0.00	0.00	3.33	0.01		0.00
P_2O_5	0.04	0.01						0.00
Fract. Solid wt.%			5.5	0.03	18.5	1.7	$\sum R^2$	**0.51**

Fractional crystallization processes

In this section the role of fractional crystallization processes in the origin of peralkaline magmas is tested with major and trace element modelling. The results of mass balance calculations are shown in Table 6. The basalt B492 was chosen as parental liquid.

The basalt-benmoreite transition can be accounted for by ~71% removal of an assemblage of olivine (~18%), clinopyroxene (~25%), plagioclase (~49%) and magnetite (~7%) ($\sum R^2$=0.33). The benmoreite-trachyte transition can be accounted for by 57 wt.% fractional crystallization of an assemblage made up of clinopyroxene (~13 wt.%), plagioclase (~77%) and magnetite (~11%) ($\sum R^2$=0.37). The transition from trachyte to rhyolite was modelled after ~26 % removal of a cumulate made up of Fe-rich olivine (~21%), alkali feldspar (~72%), magnetite (~6%) and minor clinopyroxene (<1%) ($\sum R^2$=0.51). The total fractionated assemblage to evolve the parental basaltic melt to pantelleritic compositions is roughly 90% of the original basalt melt mass, a value that is in agreement with previous estimates on similar igneous suites of MER (Peccerillo et al. 2003, 2007) and by trace element modelling reported in Fig. 5b.

Major element variations during the fractional crystallization processes have been tested also with the MELTS software (Ghiorso and Sack 1995). Since MELTS is best calibrated for basic magmas and not for evolved compositions, we modelled the fractional crystallization process only for the two first steps (from basalt to trachyte). The observed trend is reasonably well reproduced at low pressure (1 kb) and relatively low oxygen fugacity (QFM), with 1 wt.% H_2O in the starting magma. The fractionated minerals are consistent with the observed phases and with those obtained with mass balance calculations. Peccerillo et al. (2003) were able to reproduce with MELTS the liquid lines of descent to rhyolitic magmas (10% of residual liquid) for Gedemsa volcano, considering very low crystallization pressure (0.5 kb).

Fractional crystallization modelling for trace elements, using the Rayleigh equation (Fig. 5) indicate that a rhyolitic liquid is obtained after removal of about 90% of cumulates, in broad agreement with major element mass balance calculations and results on similar EARS volcanic suites (Gedemsa, Boina; Barberi et al. 1975; Peccerillo et al. 2003).

The Daly Gap problem

The bimodal chemical composition of the erupted igneous rocks, with the relative scarcity of igneous rocks with SiO_2 content between ~55 wt.% and ~65 wt.% is known as Daly Gap. This feature is observed in both continental and oceanic settings (Ferla and Meli 2006; Sheth and Melluso 2008). In the Boseti case, we can envisage a model whereby basaltic magmas were forced to evolve in at least one upper crustal magma chamber towards silicic magma compositions, and only when lighter liquids were produced (e.g., density=2.3–2.4 g/cm^3), their eruption could have taken place. Eruption of mafic liquids probably took place only in strongly extensional episodes of rifting. For this reason, the central complexes such as Boseti are predominantly formed by silicic liquids, that formed after high degrees of fractional crystallization in evolved magma reservoirs.

Crustal melting

A petrological modelling of crustal partial melting to explain the genesis of the evolved rocks can be made only with knowledge of the lithospheric structure and composition. During the last years, several geophysical, geochemical, mineralogical, and petrological studies have been carried out on the East Africa region (Tessema and Antoine 2004; Benoit et al. 2006; Furman et al. 2006a, b; Rooney et al. 2007). The Boseti Volcanic Complex is located in the northern sector of MER which is characterized by intrusion of mafic igneous rocks at shallow levels (~15–25 km deep: Mickus et al. 2007 and references therein). The basement rocks of this area are mainly Neoproterozoic to Cambrian igneous and metamorphic formations related to the Pan-African mobile belt (Peccerillo et al. 1998; Tadesse and Allen 2005; Woldemichael and Kimura 2008). The possibility that comendites and pantellerites of the Gedemsa volcano are related to partial melting of local crust has been excluded by Peccerillo et al. (2003) on the basis of simple geochemical considerations. Indeed, the local basement rocks are characterized by higher LILE/HFSE ratios compared to peralkaline magmas of Gedemsa. Partial melting of crustal rocks tends to increase the LILE/HFSE ratios in the partial melt, making unlikely the derivation of peralkaline magmas from crustal anatexis. The derivation of peralkaline rocks from non-peralkaline gabbroic rocks, representatives of basalts at depth, is also very unlikely.

Conclusions

The Boseti Volcanic Complex is located in the northern part of the Main Ethiopian Rift. It is made up by volcanic rocks with a clear bimodal chemical composition, with basic (basalts and hawaiites) and evolved types (trachytes and rhyolites of pantelleritic and comenditic affinity) and rare intermediate rocks (mugearites and benmoreites). The relatively restricted ranges of ratios between incompatible trace element ratios in basic and silicic rocks argues for relatively closed system evolutionary processes without substantial shallow depth crustal contamination. The relatively low $^{87}Sr/^{86}Sr$ (<0.7044) rules out any major role for crustal contamination in the basic rocks.

The evolved trachytes and rhyolites were likely generated by prolonged fractional crystallization processes of basaltic parental magmas in a relatively closed system at shallow depths and fO_2 conditions near the QFM buffer. The transition from basaltic to mugearitic/benmoreitic liquids can be modelled with fractional crystallization of gabbroic assemblages, whereas the transition from intermediate to silicic liquids is modelled with fractional crystallization of alkali feldspar-dominated assemblages. The peralkaline character of the evolved rocks is linked to intensive parameters (fO_2, P_{H2O}, pressure and temperature) that delayed stabilization of Na-rich mafic phases (aegirine and Na-rich amphibole) on the liquidus. In the case of the Boseti, the silicic products filled an upper crustal magma chamber (between 1.5 km and 3 km deep) and were erupted preferentially with respect to basic and intermediate products, likely hidden in deeper magma reservoirs.

Acknowledgements Pietro Brotzu (Naples), Lucio Morbidelli (Rome), Enzo Michele Piccirillo (Trieste) and Gianbosco Traversa (Rome) are gratefully thanked for their hard field work between 1970 and 1976 and for their contagious interest in the study of rift-related igneous rocks and continental flood basalts. We also wish to appreciate the contribution of Keith Bell in studying problems related to the petrogenesis of alkaline rocks throughout the world. Warm thanks are also given to Raul Carampin (Padova), Marcello Serracino (Rome) and Roberto de' Gennaro (Naples) for their help during the microprobe work. Vincenzo Morra is thanked for his precious suggestions. Lucia Civetta is thanked for the Sr-isotope determinations. This work has been supported by "fondo di Ateneo, Università di Padova" to A. Marzoli, "fondi per la Ricerca Dipartimentale" to L. Melluso and by "Fondi di Facoltà 2008" to M. Lustrino. The reviews of Andy Beard and Hetu Sheth, and the editorial comments of Lalou Gwalani were very useful for the preparation of a revised version.

References

Bailey DK, Cooper JP (1978) Comparison of the crystallisation of pantelleritic obsidians under hydrous and anhydrous condistions.

In: Progress in Experimental Petrology, NERC Publications Series 11:230–233

Baker JA, Chazot G, Menzies MA, Thirwall MF (1998) Metasomatism of the shallow mantle beneath Yemen by the Afar plume-implications for mantle plumes, flood volcanism, and intraplate volcanism. Geology 26:431–434

Barberi F, Ferrara G, Santacroce R, Treuil M, Varet J (1975) A transitional basalt- pantellerite sequence of fractional crystallization, the Boina Centre (Afar Rift, Ethiopia). J Petrol 16:22–56

Barberi F, Civetta L, Varet J (1980) Sr isotopic composition of Afar volcanics and its implication for mantle evolution. Earth Planet Sci Lett 50:247–259

Barberio MR, Donati C, Donato P, Yirgu G, Peccerillo A, Wu TW (1999) Petrology and geochemistry of Quaternary magmatism in the northern sector of the Ethiopian Rift between Debre Zeit and Awash Park. Acta Vulcanol 11:69–81

Benoit MH, Nyblade AA, VanDecar JC (2006) Upper mantle P-wave speed variations beneath Ethiopia and the origin of the Afar hotspot. Geology 34:329–332

Berhe SM, Desta B, Nicoletti M, Teferra M (1987) Geology, geochronology and geodynamic implications of the Cenozoic magmatic province in W and SE Ethiopia. J Geol Soc (Lond) 144:213–226

Bertrand H, Chazot G, Blichert-Toft J, Thoral S (2003) Implications of widespread high-μ volcanism on the Arabian Plate for Afar mantle plume and lithosphere composition. Chem Geol 198:47–61

Betton PJ, Civetta L (1984) Strontium and neodymium isotopic evidence for the heterogeneous nature and development of the mantle beneath Afar (Ethiopia). Earth Planet Sci Lett 71:59–70

Black S, Macdonald R, Kelly MR (1997) Crustal origin for peralkaline rhyolites from Kenya: evidence from U-series disequilibria and Th isotopes. J Petrol 38:277–297

Boccaletti M, Bonini M, Mazzuoli R, Abebe B, Piccardi L, Tortorici L (1998) Quaternary oblique extensional tectonics in the Ethiopian Rift (Horn of Africa). Tectonophysics 287:97–116

Boynton WV (1984) Cosmochemistry of the rare earth elements: meteorite studies. In: Henderson P (ed) Rare earth element geochemistry. Elsevier, Amsterdam, pp 63–114

Brotzu P, Morbidelli L, Piccirillo EM, Traversa G (1974) Petrological features of Boseti mountains, a complex volcanic system in the axial portion of the Main Ethiopian Rift. Bull Volcanol 38:206–234

Brotzu P, Morbidelli L, Piccirillo EM, Traversa G (1978) Geological map of Boseti Volcanic Complex (Main Ethiopian Rift). SELCA, Firenze

Brotzu P, Morbidelli L, Piccirillo EM, Traversa G (1980) Volcanological and magmatological evidence of the Boseti volcanic complex (Main Ethiopian Rift). Acc Naz Lincei (Roma) 47:317–362

Brotzu P, Morbidelli L, Piccirillo EM, Traversa G (1986) Rift structure development and magma composition in East Africa (South-East Ethiopia and East Kenya). Mem Soc Geol Ital 31:401–413

Carbonin S, Dal Negro A, Ganeo S, Piccirillo EM (1991) Influence of magma composition and oxygen fugacity on the crystal structure of C2/c clinopyroxenes from a basalt-pantellerite suite. Contrib Mineral Petrol 108:34–42

Chernet T, Hart WK, Aronson JL, Walter RC (1998) New age constraints on the timing of volcanism and tectonism in the Northern Main Ethiopian Rift-southern Afar transition zone (Ethiopia). J Volcanol Geotherm Res 80:267–280

Chorowicz J (2005) The East African Rift System. J Afr Earth Sci 43:379–410

Civetta L, D'Antonio M, Orsi G, Tilton GR (1998) The geochemistry of volcanic rocks from Pantelleria island, Sicily Channel: petrogenesis and characteristics of the mantle source region. J Petrol 39:1453–1491

Deniel C, Vidal P, Coulon C, Vellutini PJ, Piguet P (1994) Temporal evolution of mantle sources during continental rifting: the volcanism of Djibouti (Afar). J Geophys Res 99:2853–2869

Di Paola GM (1972) The Ethiopian Rift Valley (between 7°00′ and 8° 40′ lat. N). Bull Volcanol 36:517–560

Di Renzo V, Di Vito MA, Arienzo I, Carandente A, Civetta L, D'Antonio M, Giordano F, Orsi G, Tonarini S (2007) Magmatic history of Somma-Vesuvius on the basis of new geochemical and isotopic data from a deep borehole (Camaldoli della Torre). J Petrol 48:753–784

Ebinger CJ, Sleep NH (1998) Cenozoic magmatism throughout East Africa resulting from impact of a single plume. Nature 395:788–791

Ferla P, Meli C (2006) Evidence of magma mixing in the "Daly Gap" of alkaline suites: a case study from the enclaves of Pantelleria (Italy). J Petrol 47:1467–1507

Furman T, Bryce JG, Karson J, Iotti A (2004) East African Rift System (EARS) Plume structure: insight from quaternary mafic lavas of Turkana, Kenya. J Petrol 45:1069–1088

Furman T, Kaleta KM, Bryce JG, Hanan BB (2006a) Tertiary mafic lavas of Turkana, Kenya: constraints on East African plume structure and the occurrence of high-μ volcanism in Africa. J Petrol 47:1221–1244

Furman T, Bryce JG, Rooney T, Hanan BB, Yirgu G, Ayalew D (2006b) Heads and tails: 30 million years of the Afar plume. Geol Soc Spec Publ London 259:95–119

Geist D, Howard KA, Larson P (1995) The generation of oceanic rhyolites by crystal fractionation: the basalt-rhyolite association at Volcàn Alcedo, Galapagos Archipelago. J Petrol 36:965–982

George R, Rogers NW (1999) The petrogenesis of Plio–Pleistocene alkaline volcanic rocks from the Tosa Sucha region, Arba Minch, Southern Main Ethiopian Rift. Acta Vulcanol 11:121–130

George R, Rogers NW, Kelley S (1998) Earliest magmatism in Ethiopia: Evidence for two mantle plumes in one flood basalt province. Geology 26:923–926

Gibson IL (1974) A review of the geology, petrology and geochemistry of the volcano Fantale. Bull Volcanol 38:791–802

Ghiorso MS, Sack RO (1995) Chemical transfer in magmatic processes: IV. A revised and internally consistent thermodynamic model for the interpolation and extrapolation of liquid-solid equilibria in magmatic system at elevated temperatures and ressures. Contrib Mineral Petrol 119:197–212

Hart WK, Woldegabriel G, Walter RC, Mertzman SA (1989) Basaltic volcanism in Ethiopia: constraints on continental rifting and mantle interactions. J Geophys Res 94:7731–7748

Hofmann C, Courtillot V, Feraud G, Rochette P, Yirgu G, Ketefo E, Pik R (1997) Timing of the Ethiopian flood basalt event and implications for plume birth and global change. Nature 389:838–841

Justin Visentin E, Nicoletti M, Tolomeo L, Zanettin B (1974) Miocene and Pliocene volcanics of the Addis Abeba-Debra Berhan area. geo-petrographic and radiometric study. Bull Volcanol 38:237–253

Kieffer B, Arndt N, Lapierre H, Bastien F, Bosh D, Pecher A, Yirgu C, Ayalew D, Weis D, Jerram DA, Keller F, Meugniot C (2004) Flood and shield basalts from Ethiopia: magmas from the African superswell. J Petrol 45:793–834

Le Bas MJ, Le Maitre RW, Streckeisen A, Zanettin B (1986) A chemical classification of volcanic rocks based on the total alkali-silica diagram. J Petrol 27:745–750

Lepage LD (2003) ILMAT: an Excel worksheet for ilmenite–magnetite geothermometry and geobarometry. Comput Geosci 29:673–678

Lindsley DA (1971) Synthesis and preliminary results on the stability of aenigmatite ($Na_2Fe_5TiSi_6O_{20}$). Carnegie Instn Washington, Ann Rep Geophys Lab 1969–1970:188–190

Lustrino M, Morra V, Melluso L, Brotzu P, D'Amelio F, Fedele L, Franciosi L, Lonis R, Petteruti Liebercknecht AM (2004) The Cenozoic igneous acitivity of Sardinia. Per Mineral 73:105–134

Macdonald R (1974) Nomenclature and petrochemistry of the peralkaline oversaturated extrusive rocks. Bull Volcanol 38:498–516

Macdonald R, Davies GR, Bliss CM, Leat PT, Bailey DK, Smith RL (1987) Geochemistry of high-silica rhyolites, Naivasha, Kenya Rift Valley. J Petrol 28:979–1088

Macdonald R, Belkin HE, Fitton JG, Rogers NW, Nejbert K, Tindle AG, Marshall AS (2008) The roles of fractional crystallization, magma mixing, crystal mush remobilization and volatile-melt interactions in the genesis of a young basalt-peralkaline rhyolite suite, the Greater Olkaria Volcanic Complex, Kenya Rift Valley. J Petrol 49:1515–1547

Maniar PD, Piccoli PM (1989) Tectonic discrimination of granitoids. Geol Soc Am Bull 101:635–643

Merla G, Abbate E, Canuti P, Sagri M, Tacconi P (1979) Geological map of Ethiopia and Somalia. Explanatory notes. Consiglio Nazionale delle Ricerche, Italy

Mickus K, Tadesse K, Keller GR, Oluma B (2007) Gravity analysis of the Main Ethiopian Rift. J Afr Earth Sci 48:59–69

Mohr PA (1992) Nature of the crust beneath magmatically active continental rifts. Tectonophysics 213:269–284

Mohr P, Zanettin B (1988) The Ethiopian Flood basalt Province. In: Macdougall JD (ed) Continental flood basalts. Kluwer, Dordrecht, pp 63–110

Morra V, Secchi FAG, Assorgia A (1994) Petrogenetic significance of peralkaline rocks from Cenozoic calc-alkaline volcanism from SW Sardinia, Italy. Chem Geol 118:109–142

Mungall JE, Martin RF (1995) Petrogenesis of basalt-comendite and basalt-pantellerite suites, Terceira, Azores, and some implications for the origin of oceanic rhyolites. Contrib Mineral Petrol 119:43–55

Peccerillo A, Mandefro B, Solomon G, Hambisa G, Bedru H, Tesfaye K (1998) The Precambrian rocks from Southern Ethiopia: petrology, geochemistry and their interaction with recent volcanism from the Ethiopian Rift Valley. N Jb Miner Abh 173:237–262

Peccerillo A, Barberio MR, Yirgu G, Ayalew D, Barbieri M, Wu TW (2003) Relationship between mafic and peralkaline silicic magmatism in continental rift settings: a petrological, geochemical and isotopic study of the Gedemsa volcano, Central Ethiopian Rift. J Petrol 11:2003–2032

Peccerillo A, Donati C, Salto AP, Orlando A, Yirgu G, Ayalew D (2007) Petrogenesis of silicic peralkaline rocks in the Ethiopian rift: geochemical evidence and volcanological implications. J Afr Earth Sci 48:161–173

Piccirillo EM, Justin-Visentin E, Zanettin B, Joron JL, Treuil M (1979) Geodynamic evolution from plateau to rift: Major and trace element geochemistry of the central eastern Ethiopian Plateau Volcanics. N Jb Geol Palaont Abh 158:139–179

Pik R, Deniel C, Coulon C, Yirgu G, Hofmann C, Ayalew D (1998) The northwestern Ethiopian Plateau flood basalts: Classification and spatial distribution of magma types. J Volcanol Geotherm Res 81:91–111

Pik R, Deniel C, Coulon C, Yirgu G, Marty B (1999) Isotopic and trace element signatures of Ethiopian flood basalts: evidence for plume–lithosphere interactions. Geoch Cosmoch Acta 63:2263–2279

Rogers NW, Macdonald R, Fitton JG, George R, Smith M, Barreiro B (2000) Two mantle plumes beneath the East African rift System: Sr, Nd and Pb isotope evidence from Kenya Rift basalts. Earth Planet Sci Lett 176:387–400

Rooney T, Furman T, Bastow I, Ayalew D, Yirgu G (2007) Lithospheric modification during crustal extension in the Main Ethiopian Rift. J Geophys Res 112:3889–3910

Scaillet B, Macdonald R (2001) Phase relations of peralkaline silicic magmas and petrogenetic implications. J Petrol 42:825–845

Sheth HC, Melluso L (2008) The Mount Pavagadh volcanic suite, Deccan Traps: geochemical stratigraphy and magmatic evolution. J Asian Earth Sci 32:5–21. doi:10.1016/j.jsaes.2007.10.001

Sun S-S, McDonough WF (1989) Chemical and isotopic systematics of oceanic basalts: implications for mantle composition and processes. In: Saunders AD, Norry MJ (eds) Magmatism in the Ocean Basins. Geol Soc Spec Publ 42:313–345

Tadesse G, Allen A (2005) Geology and geochemistry of the Neoproterozoic Tuludimtu Ophiolite suite, Western Ethiopia. J Afr Earth Sci 41:192–211

Tessema A, Antoine LAG (2004) Processing and interpretation of the gravity field of the East African Rift: implication for crustal extension. Tectonophysics 394:87–110

Trua T, Deniel C, Mazzuoli R (1999) Crustal control in the genesis of Plio-Quaternary bimodal magmatism of the Main Ethiopian Rift (MER): geochemical and isotopic (Sr, Nd, Pb) evidence. Chem Geol 155:201–231

Vidal P, Deniel C, Vellutini PJ, Piguet P, Coulon C, Vincent J, Audin J (1991) Changes of mantle sources in the course of Rift Evolution: The Afar case. J Geophys Res 18:1913–1916

White JC, Ren M, Parker D (2005) Variation in mineralogy, temperature and oxygen fugacity in a suite of strongly peralkaline lavas and tuffs, Pantelleria, Italy. Can Mineral 43:1331–1347

Woldegabriel G, Aronson JL, Walter RC (1990) Geology, geochronology and rift basin development in the central sector of the Main Ethiopian Rift. Geol Soc Am Bull 102:439–458

Woldemichael BW, Kimura J-I (2008) Petrogenesis of the Neoproterozoic Bikilal-Ghimbi gabbro, Western Ethiopia. J Mineral Petrol Sci 102:23–46

Zanettin B, Bellieni G, Justin Visentin E (2006) New radiometric age of volcanic rocks in the central Eritrean plateau (from Asmara to Adi Quala): considerations on stratigraphy and correlations. J Afr Earth Sci 45:156–161